The role of serpentinization in magnetizing the Noachian crust of Mars

Lujendra Ojha[a, 1], **Yoann Quesnel**[b], **Alain Plattner**[c], **Suniti Karunatillake**[d], **and Sonia Tikoo**[e]

[a]Department of Earth and Planetary Sciences, Rutgers, The State University of New Jersey, Piscataway, NJ, 08854, USA. ; [b]Aix-Marseille Univ, CNRS, IRD, INRAE, CEREGE, Aix-en-Provence, France. ; [c]Department of Geological Sciences, The University of Alabama, Tuscaloosa, AL, USA. ; [d]Department of Geology and Geophysics, Louisiana State University, Baton Rouge, LA, USA; [e]Department of Geophysics, Stanford University, Stanford, CA, USA

This manuscript was compiled on May 7, 2021

Presence of a remnant crustal magnetic field and its spatial relationship to large impact basins indicates that Mars had a global dynamo during the Noachian eon (>4 Ga) (1–4). The geological processes responsible for the magnetization of the Martian crust, however, remain enigmatic. A plethora of morphological and compositional evidence suggests that high-temperature water-rock reaction was pervasive during the Noachian eon. Here we show that chemical remanent magnetization associated with serpentinization was possibly a key contributor to Mars' crustal magnetic field. The conditions in the Martian subsurface during the Noachian eon were conducive to serpentinization, as we show through numerical models of hydrothermal circulation. Geological features on Mars that implicate water-rock reaction statistically significantly align with areas showing a notably higher crustal magnetic field intensity than the average Noachian terrain. The spatial association of highest crustal magnetic field anomalies with areas of elevated heat-producing element concentrations further bolsters the likelihood of hydrothermal circulation sustained over geologic time. Such Noachian conditions would not only enable pervasive serpentinization of the mafic Martian crust but also release climate-transforming potent greenhouse gases such as H_2 and CH_4 while supporting a subsurface habitable environment.

Mars | Magnetic Field | Serpentinization

[1] The magnetic field of a planet may play a crucial role in protecting the planet's atmosphere and hydrosphere from the solar wind (5). Magnetic field records also allow us to constrain the planet's thermal evolution, as they provide a window into the past core conditions (6). While Mars no longer possesses a global source field, the Martian crust contains strong remanent magnetization, providing clear evidence for the presence of a past dynamo (1). However, the notable heterogeneity in the intensity of the crustal magnetic field (7), including complete demagnetization of the crust in some areas, suggests either substantial post dynamo modification or modification during intermittent stages of dynamo activity of the crust. Understanding the geological processes that led to the acquisition and subsequent modification of the crustal magnetic field can provide critical insight into Mars' internal, surface, and atmospheric evolution.

[2] The Martian crust is thought to have been magnetized from a source field that persisted for a few hundred million years after the planet's formation (1). However, neither the exact timing of the onset of the dynamo (2, 4, 8, 9), its structure (10), or even the mechanism by which the magnetic field was recorded (1, 11–13) are well understood. Weak crustal magnetic fields present over the hypothesized 4.5-Ga old Borealis basin and 3.7 Ga Lucus Planum have been interpreted as evidence for an early, long-lived core field on Mars (4). Competing interpretations exist for the nature of magnetization. The Martian crust possibly underwent thermoremanent magnetization (TRM) early in its history when it was cooling (1). Thus, the present-day spatial heterogeneity in the crustal field may reflect non-uniform cooling of the crust, secular variation and reversals of the dynamo, post-dynamo modification by various geological processes, or differences in depth to the magnetic source bodies. Alternatively, a single hemispheric dynamo that mostly magnetized the crust of the southern hemisphere could explain the hemispheric scale difference in the crustal magnetic field of Mars (10). Under this scenario, mainly the southern hemisphere gets magnetized, and no post-dynamo processes are required to remove the strong crustal fields in the northern hemisphere.

[3] An altogether different view posits that the acquisition of the Martian crustal magnetic field occurred primarily via chemical remanent magnetization (CRM) (12, 13). CRM results from chemical processes such as creation, modification of oxidation state, phase changes, and crustal growth of magnetic minerals at temperatures below the Curie point of the rock's magnetic carriers in the presence of a source field. A notable geological process responsible for CRM on Earth is serpentinization, a high-temperature fluid-rock reaction that occurs in ultramafic rocks of oceanic crust (14) and ophiolites (15). The serpentinization process leads to the oxidation of ferrous minerals (poor magnetic carriers) into Fe^{3+}-rich serpentines and magnetite (16), which are considered to be the most significant cause of remanent magnetization in crustal rocks on Earth (17) (and possibly Mars (18)). As a magnetic grain produced by serpentinization below its Curie point grows through a critical volume in the presence of a magnetic field,

Significance Statement

The rocks of Mars were magnetized by an Earth-like dynamo more than 4 billion years ago. However, the processes that magnetized the Martian rocks remain enigmatic. A plethora of evidence suggests the presence of substantial volumes of water in the Martian crust 4-billion years ago. Here we propose that the interaction of voluminous water with the deep crust of Mars at elevated temperatures may have been a key process that magnetized the crust. The deep rock-water reaction would not only have been notable for its role in the magnetic history of Mars but also for the biosphere and contribution of key greenhouse gases to the atmosphere.

LO conceived the project and performed all data analyses. LO wrote the paper with feedback from all other authors.

The authors declare no conflict of interest.

[1]To whom correspondence should be addressed. E-mail: luju.ojha@rutgers.edu

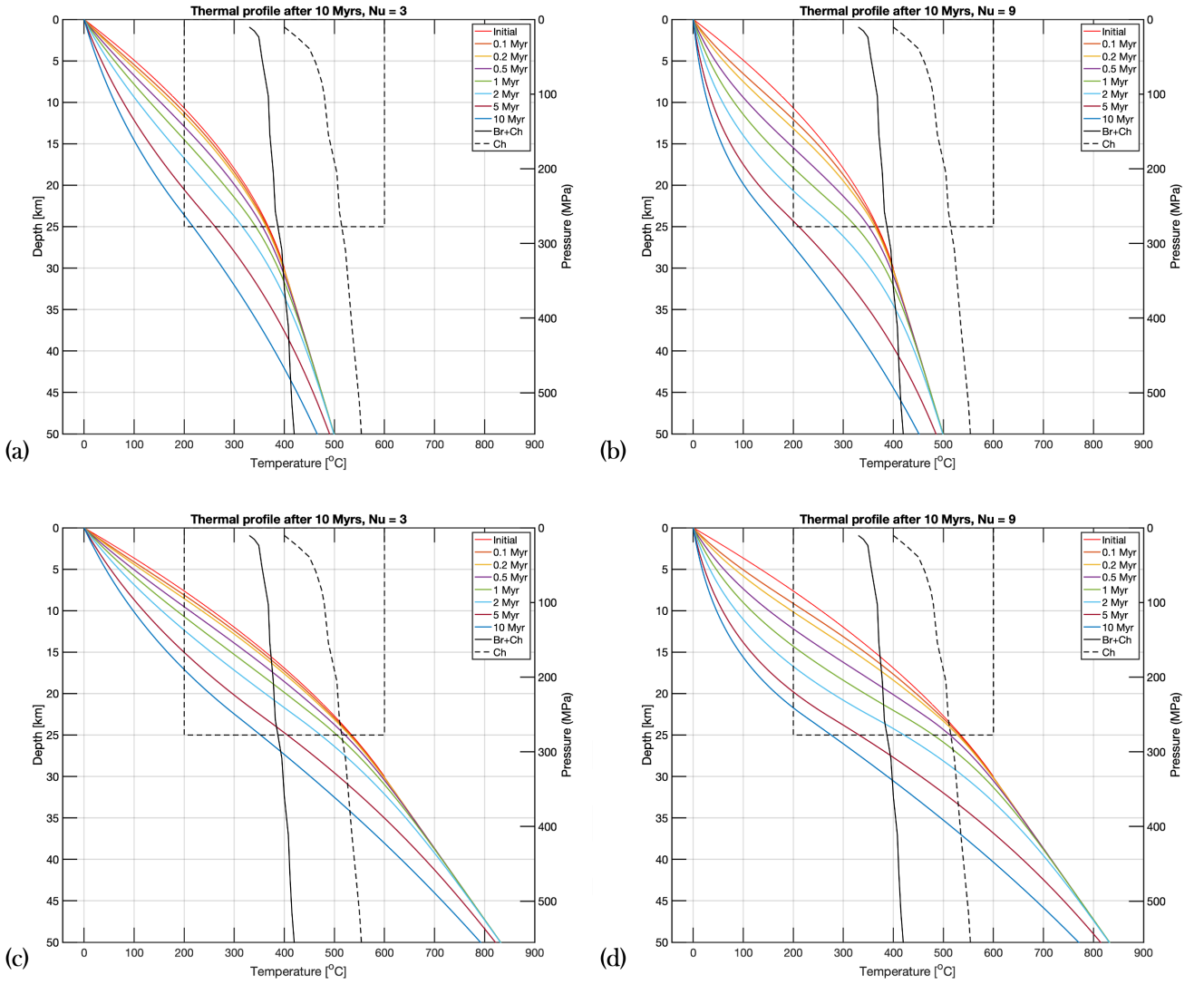

Fig. 1. Thermal profile of the Martian lithosphere after 10 Ma for a variety of Nusselt numbers. Thermal profile of the Martian lithosphere assuming a surface heat flow of 85 mW m^{-2} and Nu of 3 (a) and 9 (b). (c) and (d) Same as (a) and (b) for surface heat flow of 65 mW m^{-2}. The vertical extent of the rectangle boxes shows the range of depth where hydrothermal circulation could have occurred on Mars. The horizontal extent of the box highlights the most likely temperature range for the serpentinization reaction. The pressure-temperature equilibrium profiles for Brucite 'Br' and Chrysotile 'Ch' are also shown.

its moment becomes blocked, and it acquires a CRM.

[4] Despite being similar in efficiency to TRM (12, 13) and widespread evidence for deep aqueous alteration (19), hydrothermal circulation (20–23), and serpentinization (24) on early Mars, CRM remains poorly understood in the Martian context. CRM of the Martian crust may have been particularly important if the onset of the dynamo occurred much later in Mars' history (>500 Ma after the planet's formation, ref (8)) when the majority of the crust would have cooled past the curie temperature to allow crustal magnetic field acquisition by TRM alone. The three prime ingredients necessary for serpentinization: olivine-rich ultramafic rocks (25), liquid water (26), and high surface heat-flow (27) were readily available on Mars during the Noachian eon when the majority of the crustal magnetization is postulated to have been acquired. The highly altered nature of the Martian crust (28) further suggests that groundwater circulation could have extended to great depths (>10s km) (29). Additional evidence of serpentinization in the deep crust is provided by the spectral detection of minerals associated with serpentinization across the Noachian highlands, particularly within impact basins, through the uplift of deep crustal rocks (24, 30). Thus, serpentinization of the southern Martian crust and the subsequent CRM may explain the strong magnetic anomalies in the southern hemisphere (12, 13, 31). Here, we use numerical models of hydrothermal circulation to show that the conditions conducive to serpentinization and subsequent CRM would have been ubiquitous in the Martian subsurface during the Noachian eon. We then conduct a comprehensive spatial analysis of morphological and compositional features that implicate water-rock reactions, such as valley networks (VN) and hydrated minerals, to show that these features are preferentially located on areas of Mars with statistically higher crustal magnetic field intensity than the general Noachian terrain. We statistically confirm that

the area on Mars with the strongest crustal magnetic field intensity, Terra-Sirenum Terra-Cimmeria (TS-TC), has the highest abundance of heat-producing elements (HPE) such as Th, K, and cosmochemically equivalent U of any Noachian terrain as interpreted before (23, 32). The high abundance of HPE, capable of driving radiogenic hydrothermal systems (23), in the most magnetized region on Mars corroborates the role of hydrothermal circulation in either the initial crustal magnetization or supplementation of the TRM via CRM.

Results and Discussion

[5] The depth to which groundwater can circulate and alter the olivine-rich rocks of Mars (25) depends on the permeability profile and the brittle-ductile transition (BDT) depth of the crust. Here we consider 10^{-17} m^2 as the minimum permeability that allows hydrothermal circulation to advect heat, similar to various other terrestrial work (33, 34). The permeability profile derived from the observation of terrestrial crust (33, 34) when scaled to the lower gravity of Mars suggests that the permeability of the crust will decline from 10^{-12} m^2 at the surface to 10^{-17} m^2 at a depth of 25 km (Fig. S1). Simple scaling of hydrologic models from Earth to Mars, as we have done here, is likely an oversimplification (29); thus, we further revise the depth to which groundwater can circulate by estimating the BDT depth of the crust. The BDT temperature is set to the mean BDT temperature of non-glassy basalts 823 K (35). Beyond the BDT depth, permeability is too low for fluid to advect heat, so when the reference penetration depth (i.e., depth at which permeability exceeds 10^{-17} m^2) exceeds the BDT depth, we set the reference depth to match the BDT depth (see Methodology). This approach is similar to previous hydrological model of the Martian crust which proposed that the thickness of aquifers on Mars is controlled by the rheology of the rocks and found 26 km as the upper limit to the depth of the aquifer (29). Undoubtedly, there are uncertainties in our estimate of the maximum depth of hydrothermal circulation on Mars; however, the goal here is to examine the first order effects of hydrothermal circulation.

[6] In the presence of groundwater, various heat sources can drive hydrothermal circulation on rocky planets. Those include magmatism related to plate tectonics and mantle convection, heat provided by impact events, and radioactivity (36). Groundwater circulation, in turn, causes significant cooling of the lithosphere (34, 37, 38). We employ a one-dimensional thermal evolution model, which considers conductive heat transfer and cooling by hydrothermal circulation to constrain the conditions that could have enabled serpentinization during the Noachian eon on Mars. Similar to previous work (12), we only consider serpentinization reactions that produce magnetite (Text S1). The abundance of magnetite formed during serpentinization is controlled primarily by the reaction temperature, with higher temperature reactions usually yielding a higher volume of magnetite (39). While small amounts of magnetite can be produced in low-temperature serpentinization reactions that yield chrysotile and lizardite, voluminous magnetite via serpentinization only occurs above the lower limit of ferrous iron oxide to ferric iron oxide transformation temperature (TFFI) of 250 °C (e.g., (16)).

[7] We consider a range of surface heat flow estimates [55 – 85 mW m^{-2}] appropriate for Noachian Mars (Text S2) and run the thermal evolution model for 10 Ma to assess if conditions enabling serpentinization would have been prevalent in the Martian subsurface (Fig. 1). The vigor and the thermal effects of the hydrothermal circulation are represented by the Nusselt number (Nu), a dimensionless ratio of convective to conductive thermal flux. A Nu value of 1 implies no hydrothermal circulation, and Nu of 9 implies vigorous hydrothermal circulation. For a surface heat flow of 65 mW m^{-2} and Nu of 3, the upper 10 km of the crust could have only undergone low-temperature serpentinization. However, deeper than 10 km, the temperature exceeds the TFFI limit and could have generated voluminous magnetite (Fig. 1 a). The hydrothermal circulation would have accelerated the cooling of the crust, but even after 10 Ma, the temperature at a depth of more than 10 km would have been sufficient for serpentinization reaction to proceed. If the hydrothermal circulation was much more vigorous (e.g., Nu = 9), then the crust's accelerated cooling may have only allowed serpentinization reaction to occur for < 5 Ma (Fig. 1 b).

[8] If the surface heat flow exceeded 85 mW m^{-2}, high-temperature serpentinization could have occurred at even shallower depths (7 – 25 km), yielding serpentinized layers close to 20 km in thickness consistent with previous estimates (40, 41) (Fig. 1 c, d). The thermal profiles of the crust intercept the (pressure-temperature) P-T stability profile for both brucite + chrysotile (Text. S1) and a relatively higher temperature reaction that primarily produces chrysotile (see ref (12) for the specific chemical reactions). The limit of TFFI would have been exceeded in the Martian crust for over 10 Ma, and voluminous magnetite could have been generated in the subsurface. While the surface heat flow of Mars during the Noachian is a matter of considerable uncertainty, constraints from currently available geochemical, gravity, and topography data and thermal evolution models suggest heat flow up to 85 mW m^{-2} during the Noachian (27, 42). Even with an extremely modest surface heat flow estimate of 50 mW m^{-2}, the temperature conditions at the shallow subsurface of Mars could have allowed serpentinization reactions to progress (Fig. S2). Localized magmatic intrusions, impact heating, and volcanism would have augmented the near-surface temperature, which we do not consider here, making this endeavor a conservative approach. We also do not account for the secular cooling of the planet, which is a reasonable approach since our models only run for 10 Ma. The surface temperature (Ts) of Mars during the Noachian is a matter of considerable debate; thus, we adopt two end-member estimates of -43 °C and 0 °C. The variation in Ts does not impact the crust's deep temperature profiles or the serpentinization reaction process notably (Fig. S3). Summarily, given the currently available thermal constraints, serpentinization in the deep crust should have been ubiquitous in the Noachian highlands.

[9] Our thermal models suggest that large, regional-scale serpentinizing systems would have been prevalent mostly in the deep subsurface of Mars during the Noachian (Fig. 1). Thus, the surface detection of serpentines in present-day Mars would be limited to areas that either experienced significant excavation by geological process (e.g., impact craters) or areas that experienced added heat from magmatic intrusion, impact events, or volcanism. There is abundant spectral evidence for the presence of serpentine and serpentine+phyllosilicate mixtures across the southern highlands of Mars, although evidence for large-scale, near-surface regional serpentinization is rare

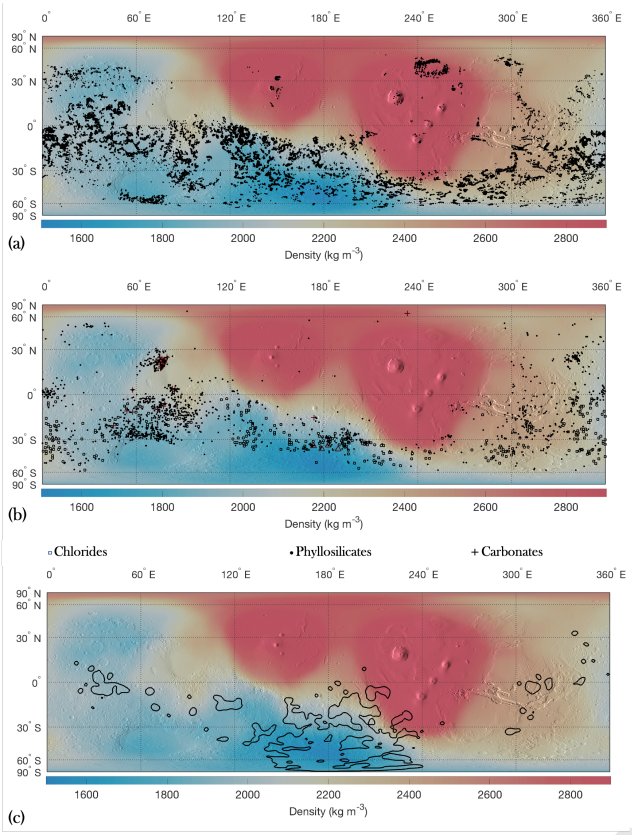

Fig. 2. Gravity derived crustal density map of Mars. (a) The distribution of valley networks overlaid on top of a gravity-derived crustal density map of Mars. (b) Same as (a) but showing the distribution of various hydrated minerals on Mars. (c) Same as (a) and (b) but the black contour lines show regions on Mars with crustal magnetic field (B) higher than 200 nT at 145 km altitude.

(24). Nevertheless, the widespread distribution of serpentine across the southern highlands suggest that serpentinization was a common process during the Noachian (24). If serpentinization was prevalent primarily in the deep crust of the southern hemisphere, it should have had a notable effect on the crustal density. The minerals associated with serpentinization can contain up to 13 wt% in water and have a low density of 2600 kg m^{-3} (39, 43). Subsequent alteration by impacts and other geological processes could have further decreased the density of the Martian southern hemisphere. A recent gravity analysis of Mars indicates a substantially lower bulk density for the southern hemispheric crust than previously assumed (44). Some regions in the southern hemisphere have estimated densities lower than 2000 kg m^{-3}, which assuming a pore-free grain density of 2600 kg m^{-3} implies a porosity of 0.23 (Fig. 2). While the crustal density map is somewhat affected by the resolution of the available gravity data (44), and thus not globally robust, it does show spatial variations of the crustal density consistent with previous findings: a generally lower density crust in the southern hemisphere when compared to the northern hemisphere (Fig. 2). The heat that drove hydrothermal circulation in the crust could have also produced enough water to erode VN (11) and form other hydrated minerals in the shallow subsurface (26). The distribution of hydrated minerals like chlorine, phyllosilicates, carbonates, and VN exhibit a broad spatial relationship with the crustal density map of Mars, preferentially forming in areas with inferred lower crustal density (Fig. 2). Notably, the area on Mars with the lowest gravity-derived density is the TS-TC region which, aside from being the most magnetized region on Mars (Fig. 2c), also contains the highest distribution of chlorides (45) and is postulated to have hosted radiogenic heat-driven hydrothermal lakes (20, 23). While we cannot prove a definitive genetic connection between the observed low crustal density and high magnetic field strength in the TS-TC region, their spatial overlap supports the notion that CRM may have played a notable role in the southern highlands. The volumetric expansion of the ultramafic layer of the Martian southern hemisphere during its serpentinization could have also caused horizontal (43) and vertical expansion of the crust (12). Previous work proposed that a net decrease in the density of the southern hemisphere and subsequent mass balance via Pratt-like isostasy could explain the topographic dichotomy between the two hemispheres of Mars (12). The widespread presence of compressional tectonic features in the southern hemisphere of Mars (46) and the thick crustal blocks postulated to occur in the TS-TC region (32) could have some genetic connection to the serpentinization of the crust.

[10] Geochemical and mineralogical observations are consistent with CRM playing a notable role, at least locally in TS-TC. Previous work noted an apparent correlation between the crustal magnetic field anomalies and the concentration of key HPE such as Th and K (e.g., (23, 32)). Radiogenic heat generated by HPE can drive amagmatic hydrothermal systems that can remain active for orders of magnitude longer (100 – 1000 Ma) than counterparts powered by alternative heat sources (47). In addition to driving serpentinization, the hydrothermal circulation of water can also differentially leach HPE from the basement rocks and enrich the surface. Previous work found that within the Noachian highlands, the highest spatially decoupled enrichment of Th and K on Mars is found in the general region of TS-TC (23, 32). On a global scale, the surface concentrations of the HPE also show a positive power-law correlation with the crustal magnetic field; however, whether this is indicative of a deep-rooted global relationship or an artifact of variable dust distribution and bias from TS-TC remains unclear (Text S3; Fig. S4; Fig. S5). Global analysis of various compositional datasets and crustal magnetization data also found evidence for compositional enhancement, related to 530 and 1000 nm due to iron bearing mineral phases at TS-TC (48).

[11] Additional insight into the possible role of CRM in the Martian magnetic field may be ascertained by examining the empirical cumulative distribution function (ECDF) of VN and hydrated minerals bearing terrain. A broad spatial correlation between the regions on Mars with high crustal remnant magnetic fields and areas hosting valley networks has been previously proposed (11). Using more recent and higher resolution data sets, including visible, infrared, and topographic data, the location of VN on Mars has been updated, yielding more than eight times as many VN on the surface of Mars as before (49) (Fig. 3). The ECDF of crustal magnetic field values from the areas bearing VN differs from the ECDF of the whole planet and Noachian terrain (Fig 4). We used a Kolmogorov–Smirnov hypothesis test (KS-test) to evaluate whether the ECDF of VN bearing terrain and Noachian terrain are from the same continuous distribution (null hypothesis)

or different continuous distribution (alternative hypothesis) at a 99% significance level. The null hypothesis fails at better than 99% confidence (p-value < 0.001). The KS-test can be modified to test whether the median values of the VN-bearing terrain are statistically higher than the crustal magnetic field values of the Noachian terrain. The modified KS-test rejects the null hypothesis in favor of the alternative hypothesis that the median crustal magnetic field values of VN bearing regions are larger than the general Noachian terrain, as also evident from Figure 4. The KS-test can produce false positives when ECDF only vary by their variance and not location (50). However, the location of the ECDF of VN is distinct from the ECDF of the Noachian terrain and all of Mars, thus the significance of our KS-test is robust. Results from unequal variance t-test between the crustal magnetic field values from the areas bearing VN and Noachian terrain also yields similar results (Table S1).

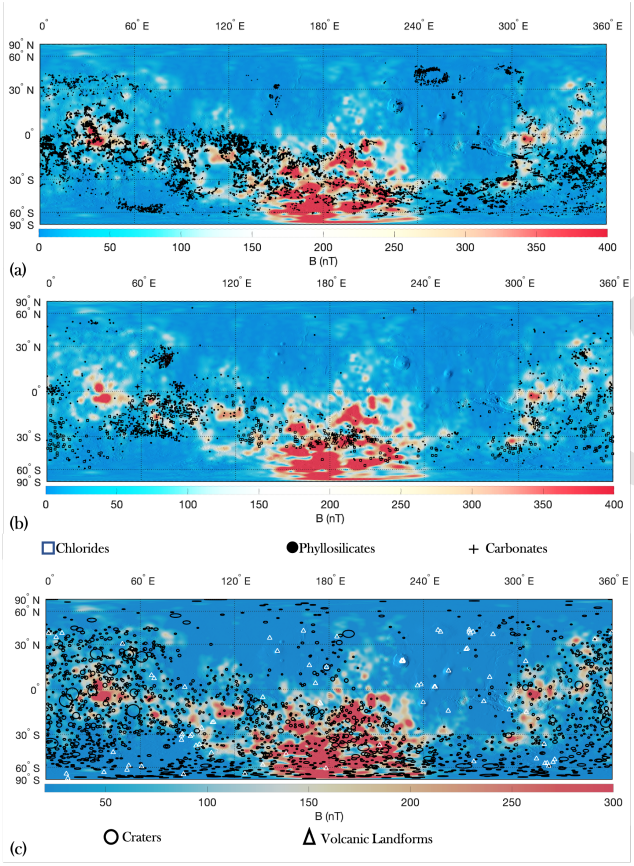

Fig. 3. The distribution of valley networks, hydrous minerals, craters, and volcanic landforms overlaid on top of a crustal magnetic field map of Mars. (a) The distribution of valley networks overlaid on top of a crustal magnetic field map of Mars. (b) The distribution of various hydrated minerals plotted on top of a crustal magnetic field map of Mars. (c) The distribution of impact craters with diameter greater than 50 km and volcanic landforms overlaid on top of a crustal magnetic field map of Mars. In all cases, the magnetic field map of Mars was computed at an altitude of 145 km above the Martian surface.

[12] A similar KS-test was used to evaluate whether the ECDF of hydrated minerals are distinct from the average Noachian terrain (Fig. 3; Fig. 4; Fig. S6). We particularly focus on the ECDF of chloride bearing regions as chlorides on Mars have been hypothesized to form as a result of the evaporation of discharged groundwater (45). The null hypothesis that the crustal magnetic field ECDF of chloride bearing regions and Noachian terrain represents the same distribution fails at better than 99% confidence ($p<0.001$) (also see Table S1). The modified KS-test also rejects the null hypothesis in favor of the alternative hypothesis that the median crustal magnetic field values of chloride bearing regions are higher than the general Noachian terrain, as also evident from Figure 4. These statistical tests suggest that VN and chlorides on Mars are preferentially located in areas of high crustal magnetic field and provides further corroboration that CRM may have played a notable role in the crustal magnetic field history of Mars. Alternatively, the putative correlations could also be explained by TRM. In this scenario, the magnetic anomalies formed due to intrusion and acquisition of thermal remnant magnetization e.g., ref (51). The heat related to the intrusion also provided enough meltwater to carve VN and allow groundwater discharge, thus explaining the putative relationship between magnetic anomalies and hydrated features (11) and potentially providing a partial solution to the faint-young sun paradox on Mars (27). However, such interpretations overlook the role of radiogenic heat that would sustain hydrothermal circulation over geologic time scales, enhancing or modulating TRM with CRM.

[13] We support our findings with a few other ECDF comparisons related to igneous intrusions, volcanic resurfacing, and impacts as processes that can elevate magnetized rock above the Curie temperature. For example, post-dynamo crustal heating by magmatic intrusion, volcanism, or impact events could have demagnetized large regions of the Martian crust (52–54). The ECDF of crustal magnetic field values from the entire planet, areas that are Noachian in surface age, areas bearing craters (diameter>50 km), and volcanic landforms are shown in Figure 4. As expected, the ECDF of the Noachian terrain is distinct from the ECDF of the entire planet as large regions of the northern hemisphere are substantially younger and weakly magnetized. The crustal magnetic field intensity ECDF of areas around craters and volcanic landforms show that these areas are notably less magnetized than the average Martian terrain and the Noachian region (Fig. 4). For example, while 60% of the Noachian terrain has crustal magnetic field values exceeding 50 nT, that corresponds to only 15% of the volcanic landforms and 30% of impact craters bearing terrain (also see Table S1). The low magnetic field values from the volcano and impact crater bearing regions on mars mean that either the magnetized layers in these areas are too thin to be resolved at the satellite altitude or that the magnetization intensity is weak.

[14] In our CRM model, the maximum depth of magnetization, based on our modeled estimate of Martian crustal permeability, Noachian heat flow, and serpentinization reaction does not exceed 25 km. This value is generally in agreement with several previous studies (55–60) that modeled the depth of the magnetic source bodies to be within the 0 - 40 km of the crust (See Table 2 by ref (12)). However, the power spectral analyses of the Martian magnetic field estimates magnetization depth up to 60 km in TS-TC (61). A key assumption in depth estimates from forward models is that the magnetic sources at depth are uniformly randomly positioned and oriented (62), which may be influenced by the possible anisotropy of the magnetic sources. Lewis and Simons

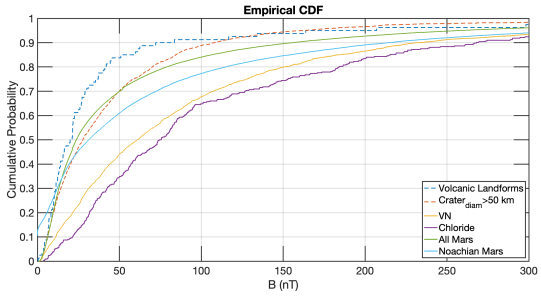

Fig. 4. An Empirical cumulative distribution function (ECDF) plot of crustal magnetic field of Mars. (a) An ECDF plot of crustal magnetic field for all of Mars, Noachian terrain, and terrain bearing VN, chlorides, impact craters, and volcanic landforms.

(2012) tested for the presence of anisotropy in both the spatial and spectral domains and found the TS-TC region to have a strong anisotropic distribution. A similar test for anisotropy in the spatial and spectral domain using Anderson-Darling test for normality in each spherical harmonic degree shows many other regions on Mars with distinct anisotropy (Fig. S7). The serpentinization reaction could also certainly exceed beyond 25 km depth and future seismic and/or gravity investigation may allow us to better constrain the depth to groundwater circulation. Here we only consider if the magnetization of the upper 25 km of the crust can explain the crustal magnetic anomalies. Using the example serpentinization reactions (Text S1; which is, on average, equivalent to R02, R14-R18 reactions of ref(11) for magnetite production), previous work ref (12) found that the magnetization intensity resulting from an Earth-like ambient surface magnetic field of 50,000 nT would range from 2 to 10-15 A/m, consistent with numerous Martian crustal magnetization models (55–60) and measurements based on meteorites (63). Thus, CRM of a 25 km thick crust can sufficiently explain the observation of the Martian crustal magnetic field.

[15] A definitive constraint on the role of CRM in the Martian crustal magnetic field history may not be possible without future sample return missions. At the present, the magnetic analysis of available Martian meteorites provide some key insight into the role of CRM in the Martian magnetic field history. The remnant magnetic field of the Martian meteorite ALH84001 resides primarily in single-domain magnetite- and pyrrhotite-bearing carbonates, the origin of which has been linked to hydrothermal activity (64). Similarly, the magnetic assemblage of the Noachian Martian breccia NWA 7034 is linked to near-surface hydrothermal alteration (65). In addition to potentially explaining the source of the magnetic field anomalies in the Martian crust,H_2 evolved from serpentinization may have supported CH_4 production via Fischer–Tropsch-type reactions in CO_2(aq) fluids (66). The thermophilic, chemoautotrophic nature of the last universal common ancestor also makes sites of subsurface water-rock reactions on Mars compelling for astrobiological exploration. This study demonstrates that conditions conducive to serpentinization would have been ubiquitous in the Martian subsurface. We show that geological features such as VN and hydrated minerals like chlorides are preferentially located on Mars in areas with higher crustal magnetic field intensity. We show that the region on Mars with the strongest crustal magnetic field also has the lowest gravity-derived crustal density and the highest enrichment of key HPE that can drive hydrothermal circulation. Collectively, our results suggest that CRM may have played a notable role in the magnetic field history of Mars, with associated sites also constituting ideal targets for exobiology missions.

Materials and Methods

Permeability Profile and Groundwater Penetration Depth. Permeability decreases with depth due to the closure of pore spaces. The permeability profile of the Martian crust is not known, so in this study, we adopt the depth-dependent permeability of (67), which was constrained by hydrological, thermal, seismic, and modeling studies in the Oregon Cascades. The permeability profile was adapted for Mars by scaling the gravity to match that of Mars:

$$K(z) = 10^{-14}\left(\frac{\frac{g_{mars}}{g_{earth}}z}{1000}\right)^{-3.2}$$

. Here, is permeability, z is depth, and gmars and gearth are the surface gravity values for Mars and Earth, respectively. Below the BDT depth, permeability is too low for fluid advection, so when the reference penetration depth (i.e., depth at which permeability exceeds 10^{-17} m^2) exceeds the BDT depth, we set the reference depth to match the BDT depth. Here we consider the BDT temperature of non-glassy basalts 823 K. The BDT depth is determined by the geothermal gradient. The permeability profile of the Martian crust likely varies from the profiles we have adopted in this work; however, the goal here is only to investigate the first-order effect of hydrothermal circulation on Mars. Further, terrestrial measurements of permeability and seismic data from InSight provide support to our permeability profile. In the young oceanic lithosphere and continental crust of Earth, the groundwater circulation depth can extend to 10 km (67). Due to reduced gravity, the confining pressure at 10 km on Earth would be reached at a much greater depth in the Martian crust. Seismic data from the InSight lander suggest that the uppermost 8 – 11 km of the present-day Martian crust is highly altered and/or fractured (28). The higher heat flow during the Noachian period would have led to annealing of the crustal porosity; thus, the depth to which groundwater could have circulated during the Noachian could have been significantly greater (68). This suggests the potential for hydraulic communications depth up to 25 km; however, below the BDT depth, permeability is too low for fluids.

Hydrothermal Circulation Model. Similar to previous work, we adopt an effective thermal conductivity λ_{eq} to account for the additional heat transfer via hydrothermal circulation (34) by linking λ_{eq} with the Nusselt number (Nu), a dimensionless number which compares the relative importance of the total heat flux (q_T) versus conductive heat flux (q_C). The governing equation for the thermal evolution is:

$$\rho C_p\left(\frac{\partial T}{\partial t} - \frac{\partial T}{\partial z}\right) = \frac{\partial}{\partial z}\lambda_{eq}\frac{\partial T}{\partial z}$$

The thermal evolution of the Martian crust and hydrothermal circulation was modeled by a previously published 1-D thermal conduction model (34).

Magnetic Analysis. The magnetic field (B) is the gradient of a scalar potential (V), which can be represented by the following spherical harmonic basis:

$$V = a\sum_{l=1}^{\infty}\left(\frac{a}{r}\right)^{l+1}\sum_{m=0}^{l}\left[g_{lm}\cos m\Phi + h_{lm}\sin m\Phi\right]P_{lm}(\cos\theta)$$

where P_{lm} are the Schmidt-normalized Legendre functions, while g_{lm} and h_{lm} are the Gauss coefficients. We use the latest scalar potential field model which combines the magnetic field data sets collected by two different spacecraft: Mars Global Surveyor (MGS) magnetometer and Mars Atmosphere and Volatile Evolution (MAVEN) magnetometer over 13 cumulative years (7). The model is expanded to degree and order 134, corresponding to a spatial resolution of

160 km. The three components of the magnetic field radial are obtained from V by the following relation:

$$B_r = -\frac{\partial V}{\partial r}$$
$$B_\theta = -\frac{\partial V}{r\partial \theta}$$
$$B_\emptyset = -\frac{-1}{r\sin(\theta)}\frac{\partial V}{\partial \theta}$$

where the

$$B_r, B_\theta, and B_\emptyset$$

represent the radial, y-direction, and x-direction components of the magnetic field. The magnetic field magnitude (B) is given by:

$$B = \sqrt{{B_r}^2 + {B_\theta}^2 + {B_\emptyset}^2}$$

We compute B at an altitude of 145 km from the surface and create cartesian maps like those shown in Figure 3.

Empirical Cumulative Distribution Function Comparison and Kolmogorov-Smirnov Test. Empirical Cumulative Distribution Functions (ECDF) for all Mars reflects all pixels from the 1x1 degree resolution crustal magnetic field map of Mars at 145 km altitude, yielding 65341 individual crustal magnetic field measurements. The ECDF for Noachian terrain reflects crustal magnetic field values of each pixel where more than 50% of the area corresponds to Noachian age. This corresponds to roughly 33100 pixels. The ECDF for VN-bearing terrain reflects the crustal magnetic field values of areas where VN lie. We use the VN database of Hynek et al. (2010) which identified 55000 individual channels and 9900 networks of channels on Mars. The hydrated minerals ECDF are created using the hydrated mineral distribution map of Ehlmann and Edwards (2014). Two spatially distinct VN or hydrated mineral deposits within the same pixel are assigned the same crustal magnetic field value. A value of 'NaN' is ascribed when the location of the VN and hydrous minerals is outside of Noachian terrain, and those sites are excluded from further statistical analysis. We use the Kolmogorov–Smirnov test (KS-test) to assess whether the probability distribution of VN and hydrated minerals bearing differ from the rest of Mars and the Noachian terrain. As a non-parametric test, an advantage of using the KS-test is that it does not require any assumption about the distribution of the data, and the results are not sensitive to the unequal sample sizes of the various probability distribution function.

Chemical Maps and Th, K Enriched Regions on Mars. We derive the regional shallow subsurface composition of the Martian crust to decimeter depths with GRS data. GRS measures the spectrum of gamma photons emitted from the Martian surface; characteristic spectral peaks from specific nuclear reactions allow the quantification of several major rock-forming elements, along with select minor and trace elements (Al, Ca, Cl, Fe, H, K, S, Si, Th)(69). Peak area above the continuum can be used to infer the percentage mass fraction (wt%) of each element over an area of the planet's surface, leading to chemical abundance maps excluding approximately latitudes beyond $\pm$ 50° where H increases rapidly.

Data Availability. All data needed to evaluate the conclusions of the paper are present in the paper, Supplementary materials, or through NASA's Planetary Data System (PDS). The Mars Odyssey Gamma Ray Spectrometer (GRS) derived chemical maps were derived from the spectral data archived at the PDS (https://pds-geosciences.wustl.edu/missions/odyssey/grs.html).

ACKNOWLEDGMENTS. We thank Sabine Stanley and Dennis Kent for reviewing the original concept.

References.

1. MH Acuña, et al., Global distribution of crustal magnetization discovered by the Mars Global Surveyor MAG/ER experiment. *Science* (1999).
2. RJ Lillis, S Robbins, M Manga, JS Halekas, HV Frey, Time history of the Martian dynamo from crater magnetic field analysis. *J. Geophys. Res. E: Planets* (2013).
3. F Vervelidou, V Lesur, M Grott, A Morschhauser, RJ Lillis, Constraining the date of the Martian dynamo shutdown by means of crater magnetization signatures. *J. Geophys. Res. Planets* **122**, 2294–2311 (2017).
4. A Mittelholz, CL Johnson, JM Feinberg, B Langlais, RJ Phillips, Timing of the martian dynamo: New constraints for a core field 4.5 and 3.7 Ga ago. *Sci. Adv.* (2020).
5. R Lundin, H Lammer, I Ribas, Planetary magnetic fields and solar forcing: Implications for atmospheric evolution. *Space Sci. Rev.* (2007).
6. D Breuer, S Labrosse, T Spohn, Thermal evolution and magnetic field generation in terrestrial planets and satellites. *Space Sci. Rev.* **152**, 449–500 (2010).
7. B Langlais, E Thébault, A Houliez, ME Purucker, RJ Lillis, A new model of the crustal magnetic field of Mars using MGS and MAVEN. *J. Geophys. Res. Planets* **124**, 1542–1569 (2019).
8. G Schubert, CT Russell, WB Moore, Timing of the Martian dynamo. *Nature* **408**, 666–667 (2000).
9. LL Hood, et al., Magnetic anomalies near Apollinaris Patera and the Medusae Fossae Formation in Lucus Planum, Mars. *Icarus* **208**, 118–131 (2010).
10. S Stanley, L Elkins-Tanton, MT Zuber, EM Parmentier, Mars' paleomagnetic field as the result of a single-hemisphere dynamo. *Science* (2008).
11. KP Harrison, RE Grimm, Controls on Martian hydrothermal systems: Application to valley network and magnetic anomaly formation. *J. Geophys. Res. E: Planets* (2002).
12. Y Quesnel, et al., Serpentinization of the martian crust during Noachian. *Earth Planet. Sci. Lett.* (2009).
13. ER Scott, M Fuller, A possible source for the Martian crustal magnetic field. *Earth Planet. Sci. Lett.* (2004).
14. PB Toft, J Arkani-Hamed, SE Haggerty, The effects of serpentinization on density and magnetic susceptibility: a petrophysical model. *Phys. Earth Planet. Interiors* **65**, 137–157 (1990).
15. D Bonnemains, et al., Magnetic signatures of serpentinization at ophiolite complexes. *Geochem. Geophys. Geosystems* (2016).
16. M Andreani, M Muñoz, C Marcaillou, A Delacour, μXANES study of iron redox state in serpentine during oceanic serpentinization. *Lithos* **178**, 70–83 (2013).
17. DJ Dunlop, Ö Özdemir, *Rock magnetism: fundamentals and frontiers*. (Cambridge university press) No. 3, (2001).
18. DJ Dunlop, J Arkani-Hamed, Magnetic minerals in the Martian crust. *J. Geophys. Res. Planets* **110** (2005).
19. BL Ehlmann, et al., Subsurface water and clay mineral formation during the early history of Mars. *Nature* **479**, 53–60 (2011).
20. JR Michalski, EZ Dobrea, PB Niles, J Cuadros, Ancient hydrothermal seafloor deposits in Eridania basin on Mars. *Nat. Commun.* (2017).
21. BL Ehlmann, et al., Orbital identification of carbonate-bearing rocks on Mars. *Sci. (New York, N.Y.)* **322**, 1828–1832 (2008).
22. CE Viviano, JE Moersch, HY McSween, Implications for early hydrothermal environments on Mars through the spectral evidence for carbonation and chloritization reactions in the Nili Fossae region. *J. Geophys. Res. Planets* **118**, 1858–1872 (2013).
23. L Ojha, S Karunatillake, S Karimi, J Buffo, Amagmatic hydrothermal systems on Mars from radiogenic heat. *Nat. Commun.* **12**, 1754 (2021).
24. ES Amador, JL Bandfield, NH Thomas, A search for minerals associated with serpentinization across Mars using CRISM spectral data. *Icarus* (2018).
25. VE Hamilton, HY McSween, B Hapke, Mineralogy of Martian atmospheric dust inferred from thermal infrared spectra of aerosols. *J. Geophys. Res. E: Planets* **110**, 1–11 (2005).
26. BL Ehlmann, CS Edwards, Mineralogy of the Martian Surface. *Annu. Rev. Earth Planet. Sci* **42**, 291–315 (2014).
27. L Ojha, J Buffo, S Karunatillake, M Siegler, Groundwater production from geothermal heating on early Mars and implication for early martian habitability. *Sci. Adv.* **6** (2020).
28. P Lognonné, et al., Constraints on the shallow elastic and anelastic structure of Mars from InSight seismic data. *Nat. Geosci.* (2020).
29. JC Hanna, RJ Phillips, Hydrological modeling of the Martian crust with application to the pressurization of aquifers. *J. Geophys. Res. E: Planets* (2005).
30. J Carter, F Poulet, JP Bibring, N Mangold, S Murchie, Hydrous minerals on Mars as seen by the CRISM and OMEGA imaging spectrometers: Updated global view. *J. Geophys. Res. E: Planets* **118**, 831–858 (2013).
31. RJ Lillis, HV Frey, M Manga, Rapid decrease in Martian crustal magnetization in the Noachian era: Implications for the dynamo and climate of early Mars. *Geophys. Res. Lett.* (2008).
32. S Bouley, et al., A thick crustal block revealed by reconstructions of early Mars highlands. *Nat. Geosci.* (2020).
33. CE Manning, SE Ingebritsen, Permeability of the continental crust: Implications of geothermal data and metamorphic systems. *Rev. Geophys.* (1999).
34. W Cao, CTA Lee, J Yang, AV Zuza, Hydrothermal circulation cools continental crust under exhumation. *Earth Planet. Sci. Lett.* (2019).
35. M Violay, et al., An experimental study of the brittle-ductile transition of basalt at oceanic crust pressure and temperature conditions. *J. Geophys. Res. Solid Earth* (2012).
36. CR German, KL Von Damm, 6.07 - Hydrothermal Processes, eds. HD Holland, KKBTToG Turekian. (Pergamon, Oxford), pp. 181–222 (2003).
37. CR Lister, Heat flow and hydrothermal circulation. *Annu. review earth planetary sciences: volume 8* (1980).
38. H Kooi, Groundwater flow as a cooling agent of the continental lithosphere. *Nat. Geosci.* (2016).
39. F Klein, et al., Magnetite in seafloor serpentinite—Some like it hot. *Geology* **42**, 135–138 (2014).
40. E Chassefière, B Langlais, Y Quesnel, F Leblanc, The fate of early Mars' lost water: the role of serpentinization. *J. Geophys. Res. Planets* **118**, 1123–1134 (2013).
41. J Lasue, Y Quesnel, B Langlais, E Chassefière, Methane storage capacity of the early martian cryosphere. *Icarus* (2015).
42. AC Plesa, et al., How large are present-day heat flux variations across the surface of Mars? *J. Geophys. Res. Planets* (2016).
43. L Eppelbaum, I Kutasov, A Pilchin, *Applied geothermics*. (Springer), (2014).
44. S Goossens, et al., Evidence for a low bulk crustal density for Mars from gravity and topography. *Geophys. Res. Lett.* **44**, 7686–7694 (2017).

45. TD Glotch, JL Bandfield, LL Tornabene, HB Jensen, FP Seelos, Distribution and formation of chlorides and phyllosilicates in Terra Sirenum, Mars. *Geophys. Res. Lett.* (2010).
46. K Mueller, M Golombek, Compressional structures on Mars (2004).
47. J Brugger, PA Wülser, J Foden, Genesis and preservation of a uranium-rich Paleozoic epithermal system with a surface expression (northern Flinders Ranges, South Australia): Radiogenic heat driving regional hydrothermal circulation over geological timescales. *Astrobiology* **11**, 499–508 (2011).
48. A AlHantoobi, J Buz, JG O'Rourke, B Langlais, CS Edwards, Compositional Enhancement of Crustal Magnetization on Mars. *Geophys. Res. Lett.* **n/a**, e2020GL090379 (2020).
49. BM Hynek, M Beach, MRT Hoke, Updated global map of Martian valley networks and implications for climate and hydrologic processes. *J. Geophys. Res.* (2010).
50. GJ Filion, The signed Kolmogorov-Smirnov test: Why it should not be used (2015).
51. F Nimmo, Dike intrusion as a possible cause of linear Martian magnetic anomalies. *Geology* **28**, 391–394 (2000).
52. RJ Lillis, J Dufek, JE Bleacher, M Manga, Demagnetization of crust by magmatic intrusion near the Arsia Mons volcano: Magnetic and thermal implications for the development of the Tharsis province, Mars. *J. Volcanol. Geotherm. Res.* **185**, 123–138 (2009).
53. PS Mohit, J Arkani-Hamed, Impact demagnetization of the martian crust. *Icarus* (2004).
54. P Rochette, et al., High pressure magnetic transition in pyrrhotite and impact demagnetization on Mars. *Geophys. Res. Lett.* **30** (2003).
55. JE Connerney, et al., Magnetic lineations in the ancient crust of Mars. *Science* (1999).
56. KF Sprenke, LL Baker, Magnetization, Paleomagnetic Poles, and Polar Wander on Mars. *Icarus* (2000).
57. JJ Frawley, PT Taylor, Paleo-pole positions from martian magnetic anomaly data. *Icarus* (2004).
58. J Arkani-Hamed, Thermoremanent magnetization of the Martian lithosphere. *J. Geophys. Res. E: Planets* (2003).
59. B Langlais, M Purucker, M Mandea, Crustal magnetic field of Mars. *J. Geophys. Res.* **109**, 2008 (2004).
60. KA Whaler, ME Purucker, A spatially continuous magnetization model for Mars. *J. Geophys. Res. E: Planets* (2005).
61. KW Lewis, FJ Simons, Local spectral variability and the origin of the Martian crustal magnetic field. *Geophys. Res. Lett.* (2012).
62. CV Voorhies, TJ Sabaka, M Purucker, On magnetic spectra of Earth and Mars. *J. Geophys. Res. E: Planets* (2002).
63. P Rochette, et al., Matching Martian crustal magnetization and magnetic properties of Martian meteorites. *Meteorit. Planet. Sci.* (2005).
64. AH Treiman, HE Amundsen, DF Blake, T Bunch, Hydrothermal origin for carbonate globules in Martian meteorite ALH84001: A terrestrial analogue from Spitsbergen (Norway). *Earth Planet. Sci. Lett.* (2002).
65. J Gattacceca, et al., Martian meteorites and Martian magnetic anomalies: A new perspective from NWA 7034 (2014).
66. C Oze, M Sharma, Have olivine , will gas : Serpentinization and the abiogenic production of methane on Mars. **32**, 10–13 (2005).
67. MO Saar, M Manga, Depth dependence of permeability in the Oregon Cascades inferred from hydrogeologic, thermal, seismic, and magmatic modeling constraints. *J. Geophys. Res. Solid Earth* (2004).
68. S Gyalay, F Nimmo, AC Plesa, M Wieczorek, Constraints on Thermal History of Mars From Depth of Pore Closure Below InSight. *Geophys. Res. Lett.* (2020).
69. WV Boynton, et al., Concentration of H, Si, Cl, K, Fe, and Th in the low- and mid-latitude regions of Mars. *J. Geophys. Res. E: Planets* **112** (2007).